Available online at www.sciencedirect.com
SCIENCE DIRECT®
Lithos 66 (2003) 23–36
LITHOS
www.elsevier.com/locate/lithos

First report of early Triassic A-type granite and syenite intrusions from Taimyr: product of the northern Eurasian superplume?

Valery A. Vernikovsky[a,*], Victoria L. Pease[b], Antonina E. Vernikovskaya[a], Andrey P. Romanov[c], David G. Gee[d], Alexey V. Travin[a]

[a] *United Institute of Geology, Geophysics and Mineralogy, Siberian Branch, Russian Academy of Sciences, Koptyug Prosp., 3, 630090 Novosibirsk, Russia*
[b] *Institute for Geology and Geochemistry, Stockholm University, SE-10691 Stockholm, Sweden*
[c] *Institute of Geology and Mineral Raw Materials, Mira Street, 55, 660049 Krasnoyarsk, Russia*
[d] *Department of Earth Sciences, Uppsala University, Villavagen 16, SE-75236 Uppsala, Sweden*

Received in revised form 21 May 2001; accepted 10 July 2002

Abstract

Ion-microprobe U–Th–Pb analyses of zircon from three high-level syenite–granite stocks in the western part of the Taimyr fold-and-thrust belt have yielded early Triassic ages of 249–241 Ma. Those syenite–granite bodies intrude unmetamorphosed late Paleozoic to early Mesozoic terrigenous and volcanic supracrustal rocks, including the early Triassic Siberian traps. $^{40}Ar-^{39}Ar$ isotopic ages of 245–233 Ma correlate well with the ion-microprobe data and define the time of closure for the K–Ar isotopic system. Limited geochemical data for the early Triassic syenite–granite plutons show that they have metaluminous compositions, high potassium, high REE and high LIL concentrations, and $^{87}Sr/^{86}Sr$ and ε_{Nd} ratios intermediate between crust and mantle, suggesting a hybrid mantle–crustal origin. We tentatively suggest that they formed in an anorogenic setting as a result of the Permo-Triassic Euroasian superplume.

Keywords: Arctic Siberia; Taimyr; Early Triassic; Plume magmatism; Syenite–granite; U–Pb and Ar–Ar geochronology

1. Introduction

Many researchers have considered the widespread Permo-Triassic magmatism of northern Eurasia to be a reflection of a plume or superplume (Sharma et al., 1992; Sharma, 1997; Dobretsov, 1997; Yarmolyuk et al., 1997; Zolotukhin, 1998; Dobretsov and Vernikovsky, 2001). The Siberian trap area (also referred to as the Siberian Flood Basalt Province) is one of the largest known regions of plume magmatism in terms of the volume of magmatic products (basalt, tuff, dolerite and other associated rock types). Permo-Triassic trap magmatism is widely distributed on the Siberian platform (Zolotukhin, 1998), beneath a cover of Mesozoic–Cenozoic deposits in the West Siberian basin and in the southeastern Kara Sea (Dobretsov, 1997; Bogdanov et al., 1998), and also on the Taimyr Peninsula (Ravich and Chaika, 1956; Vakar, 1962; Bezzubtsev et al., 1986, Vernikovsky, 1996). Similar

* Corresponding author.
E-mail addresses: taimyr@uiggm.nsc.ru (V.A. Vernikovsky), vicky.pease@nrm.se (V.L. Pease), gee@geofys.uu.se (D.G. Gee).

0024-4937/02/$ - see front matter © 2002 Elsevier Science B.V. All rights reserved.
PII: S0024-4937(02)00192-5

to other magmatic provinces fed by mantle plumes, the Siberian traps were formed over a short period, mainly between 250 and 245 Ma (Campbell et al., 1992; Basu et al., 1995; Dalrymple et al., 1995; Renne et al., 1995; Sharma, 1997; Yarmolyuk et al., 1997). The oldest U–Pb age for Siberian flood-basalt volcanism was obtained by Kamo et al. (1996), who published a precise U–Pb zircon and baddeleyite age for the Noril'sk 1 leucogabbro of 251.2 ± 0.3 Ma, which intrudes into the latter trap volcanic rocks. This age is within error of the estimated age for the Permo-Triassic boundary, 251 ± 3.6 Ma (Claoué-Long et al., 1991).

Alkaline and subalkaline granitoid magmatism of this age is also well documented in Permo-Triassic accretionary–collisional complexes surrounding the southern Siberian traps (Jahn et al., 1990; Yarmolyuk et al., 1997). It has been suggested that these young hot rocks were susceptible to partial melting after the onset of plume magmatism (Dobretsov, 1997).

On the Taimyr Peninsula and nearby islands in the Kara Sea, small bodies of monzonite, syenite and subalkaline and alkaline granite are present. On the basis of geological arguments, their age has been defined as post-Permian but pre-Cretaceous (Ravich and Chaika, 1959; Egiazarov, 1959; Vakar, 1962; Pogrebitsky, 1971; Bezzubtsev et al., 1986). Some researchers considered their formation to be a result of trap magmatism via the assimilation of host rocks by basic magma (Vakar, 1962) or anatexis of roof pendent by superheated basic magma (Zolotukhin, 1990). We present new petrologic, geochemical and geochronological results from syenite–granite massifs in northwestern Taimyr that provide new evidence in support of their association with the Permo-Triassic trap magmatism of the north Euroasian superplume.

2. Geological setting

The Uboininsky, Rastorguev, Morzhov and other syenite and granite bodies generally form small stocks (up to 20–35 km^2) intruding Precambrian to Early Triassic lithologies of the Kara block, Central Taimyr accretionary belt and the South Taimyr fold belt (Vernikovsky, 1996). They are widespread in the western region, mainly being emplaced into late Carboniferous, Permian and early Triassic terrigenous volcano-sedimentary and volcanogenic rocks of the South Taimyr fold belt (Figs. 1 and 2). Here, Devonian and early Carboniferous carbonate rocks (limestone and dolostone) form the cores and slopes of small anticlines. Up-section carbonate rocks give way to terrigenous material. This mid-Carboniferous change in the sedimentation regime (Pogrebitsky, 1971; Bezzubtsev et al., 1986) has been correlated with the beginning of the Kara orogeny in northern Taimyr (Vernikovsky, 1995; Vernikovsky et al., 1995, 1998). For example, in the Makarovskaya Group, limestone gives way to rhythmically interstratified argillite, siltstone and sandstone, which resemble a flysch sequence. In late Carboniferous strata, the volume of sandstone increases to 30–65% and carbonates are reduced to a few percent of the succession. Coal becomes common in the Permian. At the end of the Upper Permian, polymict conglomerate with metamorphic, igneous and carbonate fragments, and coarse sandstone, which varies in color from greenish-gray to reddish-gray, are typical (Bezzubtsev et al., 1986; Vladimirov and Nikulov, 1991). This suggests that deposition progressed from a lagoonal to a continental setting. In the latest Permian and early Triassic, subalkaline mafic lavas (the Syrodayskaya and Labanskaya Formations) become abundant. These formations include basalt, trachibasalt, leucobasalt, tuff, tuffaceous sandstone and polymict and volcanogenic sandstone. In addition to trap volcanic rocks, dolerite sills and dykes up to tens of kilometers wide and up to hundreds of kilometers long are common in the region.

Granite and syenite bodies of diverse composition intrude the late Carboniferous and Permian (mainly terrigenous) deposits, and display contact metamorphic aureoles less than 100 m wide. They also intrude the Permo-Triassic extrusive and intrusive rocks associated with the Siberian traps (Fig. 2). Given the unmetamorphosed country rocks, it is evident that the syenite–granite bodies are high-level intrusions.

3. Petrography

The intrusions comprise syenite, quartz syenite, quartz monzonite, subalkaline granite and subordinate alkaline syenite and granite. Of these, syenite and

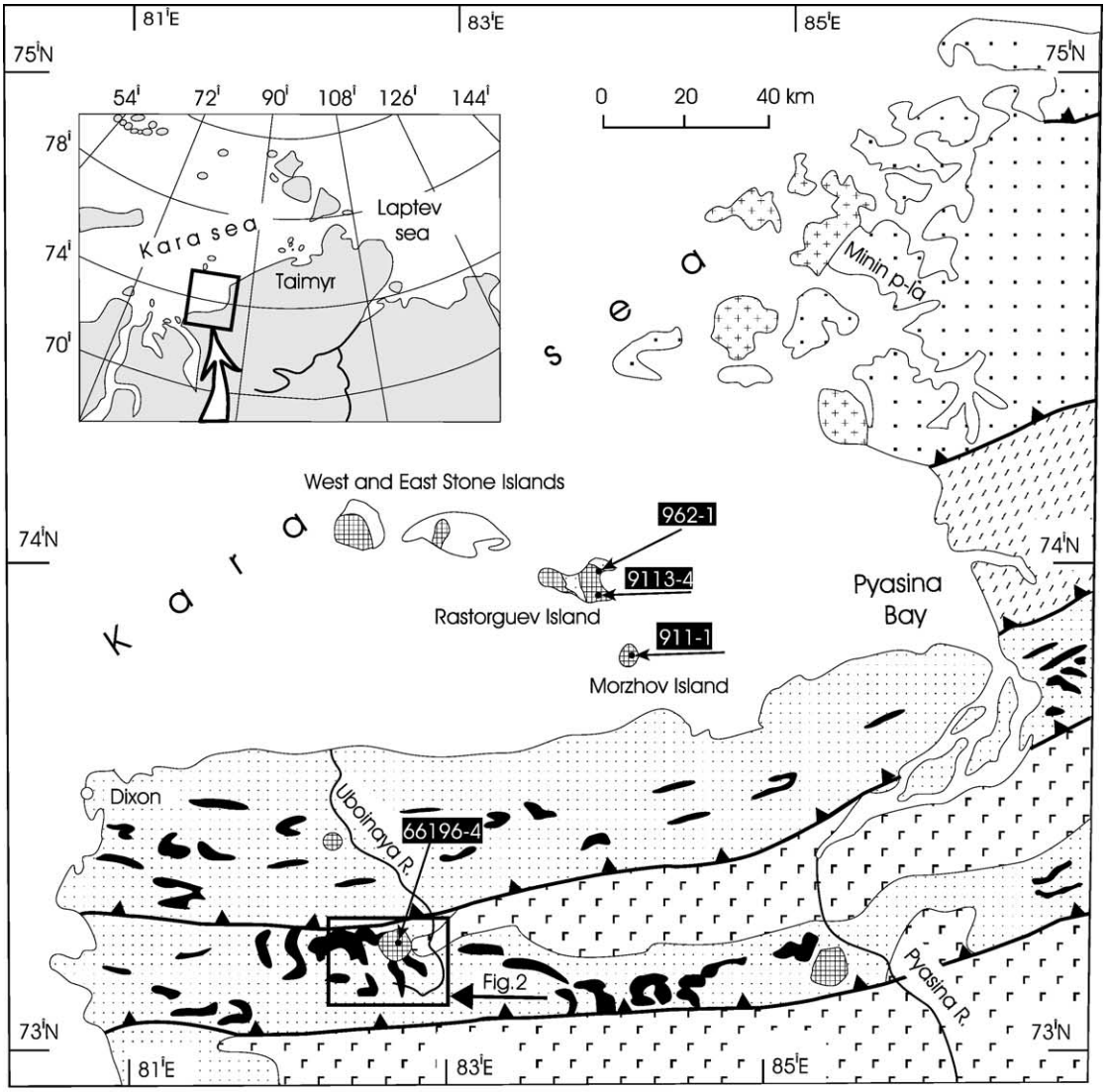

Flyschoid deposits, Kara block (NP-Cambrian)

Cover, Central Taimyr accretionary block (V-PZ)

Essentially terrigenous deposits, South Taimyr foldbelt (C-P)

Calc-alkaline granite (300-264 Ma)

Basalt, tuff (T_1)

Dolerite (T_1)

Syenite, monzonite, subalkaline and alkaline granite (T_1)

Thrusts

911-1 Sampling point

Fig. 1. Geological map of northwest Taimyr.

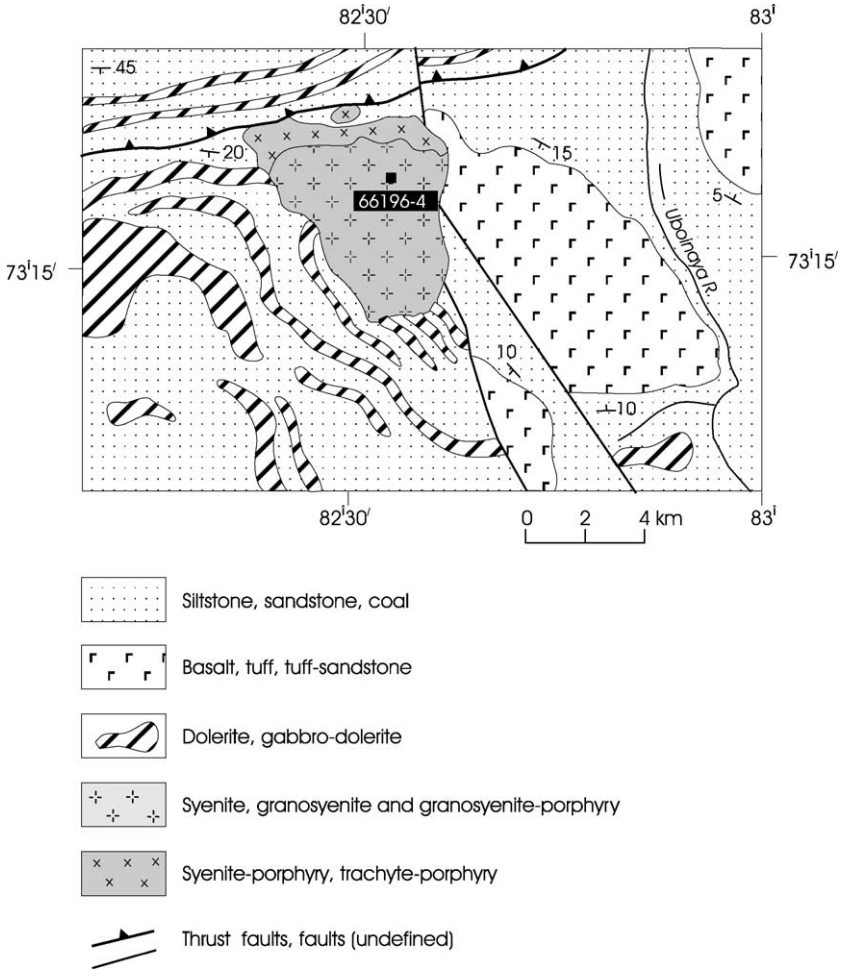

Fig. 2. Geological map near the Uboinaya River region.

quartz syenite are the most widespread and voluminous (Ravich and Chaika, 1959). They are generally greenish-gray and pinkish-gray porphyritic rocks, with 1–4 cm phenocrysts of idiomorphic plagioclase and hypidiomorphic potassium feldspar in a medium- to fine-grained groundmass. Plagioclase (commonly andesine) and potassium feldspar (orthoclase) are typically in approximately equal proportions or the latter predominates. Mafic minerals include biotite and hornblende, which do not exceed 10–15%, and minor pyroxene. Pyroxene is augite, aegirine–augite and rarely diopside. Accessory minerals include titanite, apatite, magnetite, titanomagnetite, allanite, zircon and fluorite. Chlorite, actinolite, epidote and calcite are secondary minerals.

Biotite and amphibole, commonly idiomorphic, contain inclusions of titanomagnetite, feldspar, apatite, titanite and fluorite. Plagioclase is normally zoned with saussuritized cores and albite rims. Plagioclase phenocrysts are antiperthitic and show albite, carlsbad and pericline twinning. Plagioclase forms myrmekite where in contact with orthoclase and is locally mantled by orthoclase rims with inclusions of mafic minerals, titanite, apatite, fluorite and plagioclase. Xenomorphic crystal shape and microperthite texture are typical for orthoclase. The large quantity of fluorine-bearing inclusions and the high CaO in these rocks (Table 1) suggest that fluorite and other fluorine-bearing minerals were stable under these high-level conditions and crystallized as magmatic miner-

Table 1
Chemical composition of the rocks of subalkaline series from northern Taimyr

Sample	962-1 (1)	9113-4 (2)	66196-4 (3)	911-1 (4)
SiO_2 (wt.%)	57.18	57.79	63.82	67.99
TiO_2	0.57	0.65	0.58	0.33
Al_2O_3	18.35	15.7	15.27	15.24
Fe_2O_3	5.73	6.02	3.54	2.91
MnO	0.14	0.15	0.12	0.12
MgO	2.76	3.23	2.2	1.13
CaO	4.57	6.11	2.82	2.65
Na_2O	3.25	2.94	3.53	3.48
K_2O	6.03	6.04	5.25	5.07
P_2O_5	0.46	0.5	0.24	0.15
LOI	0.92	0.82	0.58	0.9
Li (ppm)	39.3	21.6	17.2	21.3
Sc	9.02	15.2	6.65	5.06
V	73	108	38.3	33.7
Cr	43.2	99.3	96.5	23.9
Co	13.6	16.3	7.77	5.59
Ni	19.9	33.1	42.9	15.3
Cu	21.2	80.1	21.3	6.83
Zn	71.8	74.6	34.4	26.7
Ga	18.8	19.8	17.1	18.4
Rb	187	201	156	199
Sr	1695	2793	668	913
Y	22.4	28.1	11.2	14.5
Zr	208	126	188	176
Nb	16.3	15.4	16.3	17
Cs	8.51	4.38	2.08	3.94
Ba	3280	5841	1215	1944
La	67.7	90.8	42.7	45.6
Ce	110	161	49.7	65.8
Pr	15.6	21.4	10.5	9.66
Nd	58.6	79.2	40.1	18.6
Sm	9.4	13.6	5.9	4.3
Eu	3.12	4.22	1.39	1.69
Gd	8.01	12	4.37	4.62
Tb	0.84	1.27	0.45	0.54
Dy	3.99	5.54	2.26	2.51
Ho	0.711	0.951	0.372	0.51
Er	1.92	2.13	1.07	1.23
Tm	0.26	0.32	0.17	0.21
Yb	2.14	2.22	1.08	1.54
Lu	0.253	0.275	0.135	0.215
Hf	4.3	3.89	5.08	5.17
Ta	0.78	0.75	0.96	1.19
Pb	54.8	69.8	20.4	36.5
Th	23.1	38	22.2	33.3
U	2.67	3.95	1.42	1.07
$(Ce/Yb)_{CN}$	51.40	72.52	46.02	42.73

Whole-rock analyses on trace and rare-earth elements were prepared by ICP-MS method using a VG Element PQ2 ICP-MS mass spectrometer. Sm and Nd contents were determined by isotope dilution. (1 and 2) Syenite (Rastorguev Island), (3) syenite–porphyry (Uboinaya River), (4) granosyenite (Morzhov Island). $(Ce/Yb)_{CN}$: normalizing values after Evensen et al. (1978).

als. Experimental results have shown that primary magmatic fluorite and titanite are stable in melts at 850 °C and 200 MPa in some metaluminous, A-type granites (Price et al., 1999).

4. Major and trace element geochemistry

Whole-rock analyses for four samples from the Uboininsky, Rastorguev and Morzhov bodies are listed in Table 1 and are plotted in Figs. 3 and 4. Analyses of major elements were carried out at the United Institute of Geology, Geophysics and Mineralogy, Novosibirsk, Russia, by X-ray fluorescence. Trace and rare-earth elements were measured by ICP-MS using a VG Element PQ2 ICP-MS mass spectrometer at the Institute of Precambrian Geology and Geochronology, St. Petersburg, Russia. Owing to the limited number of available samples, the conclusions must be regarded as tentative, although the samples are considered to be representative of the bodies.

SiO_2 varies from 57.2 to 68 wt.%, K_2O from 5 to 6 wt.%, K_2O/Na_2O ratio = 1.–2.1 and $FeO^T/MgO = 1.4–2.3$. These rocks are metaluminous (Shand, 1943), with low $Al_2O_3/CaO + Na_2O + K_2O$ (mol%) ratios of 0.7–0.95. They are subalkaline and contain normative diopside (0.43–10.56%) and hypersthene (2.64–6.67%). They have high Ga/Al ratios ($Ga/Al \times 10^4 = 1.9–2.4$) and elevated Rb and Nb concentrations (Fig. 4). These are characteristic features of A-type granitoids (Collins et al., 1982). All samples are also characterized by high Sr (668–2793 ppm) and very high Ba (1215–5841 ppm) (Fig. 4), and lack, or have weak, negative Eu anomalies (Fig. 3). Light rare-earth elements (LREE) are enriched relative to heavy rare-earth elements (HREE) with $(Ce/Yb)_{\tilde{N}N} = 42.7–72.5$ (Fig. 4). The significant increase of LREE relative to HREE in these rocks is inferred to be due to the incompatible behavior of large ion lithophile components in mafic magma compared to melts with higher SiO_2 (Collins et al., 1982). With increased silica, minerals with elevated REE, such as titanite, apatite and allanite, crystallize out of the melt consistent with the observed REE distributions (Fig. 3). Σ_{REE} decreases from 364.9 to 157 ppm from mafic to felsic compositions. In the samples with relatively high silica, a small negative

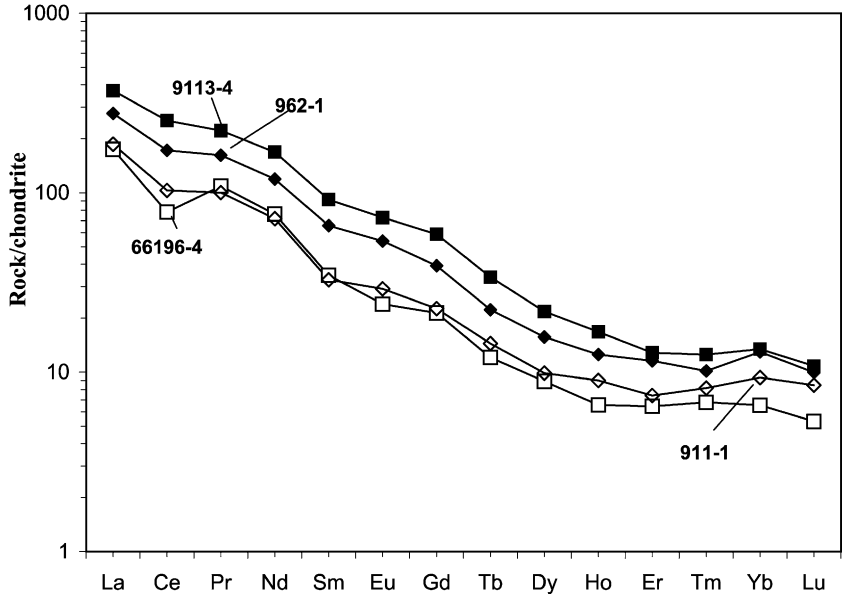

Fig. 3. Distribution diagram of rare earth elements normalized to chondrite (Evensen et al., 1978) for the rocks of subalkaline series from northwest Taimyr.

Ce anomaly is present, testifying to significant Ce fractionation in the most differentiated melts with lower contents of trace and RE elements (Fig. 3). The HREE contents of the subalkaline samples are similar to those of average ocean ridge granite (ORG), so depleted mantle is considered to be the probable

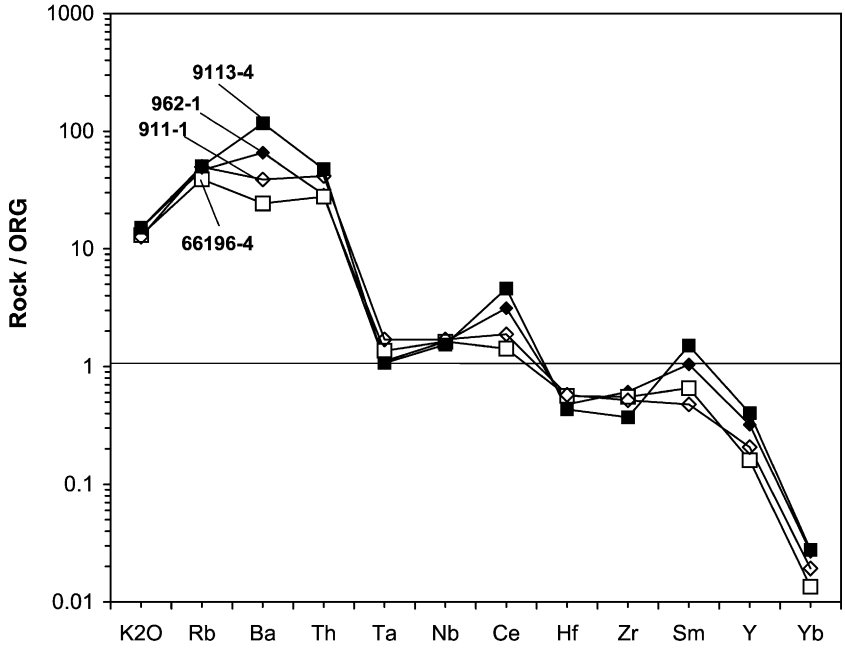

Fig. 4. Multicomponent diagram for the rocks of subalkaline series from northwest Taimyr. Element contents are normalized to ORG (Pearce et al., 1984).

Table 2
U–Th–Pb ion-microprobe analytical data

Sample (grain spot)	U (ppm)	Th (ppm)	Pb (ppm)	Th/U	f_{206} (%)	$^{207}Pb/^{206}Pb$	±1σ (%)	$^{206}Pb/^{238}U$	±1σ (%)	Age estimates (Ma) $^{207}Pb/^{206}Pb$	Age estimates (Ma) $^{206}Pb/^{238}U$	Disc. (%)
66196-4 Syenite												
1.1c	586	935	47	(0.223)	15.00	0.16690	0.92	0.04279	5.66	2526.8 ± 15.4	270.1 ± 15.0	− 86.5
2.1c	420	487	23	1.201	0.16	0.05099	1.57	0.03754	5.67	240.4 ± 35.7	237.6 ± 13.2	
2.2r	643	423	32	0.631	0.17	0.05167	1.33	0.03883	5.67	270.8 ± 30.1	245.6 ± 13.7	
3.1c	267	269	14	1.268	1.20	0.05023	2.19	0.03625	5.66	205.7 ± 49.9	229.5 ± 12.8	
3.2c	300	415	17	1.118	0.34	0.05193	1.45	0.03787	2.30	282.3 ± 32.8	239.6 ± 5.4	
4.1c	135	152	8	(0.595)	0.85	0.05706	2.85	0.03960	5.65	493.9 ± 61.6	250.4 ± 13.9	− 15.0
5.1c	710	992	40	1.324	0.45	0.05181	1.37	0.03666	5.65	277.0 ± 31.1	232.1 ± 12.9	
5.2c	613	782	40	0.181	10.65	0.13410	1.32	0.03903	2.54	2152.3 ± 22.9	246.8 ± 6.1	− 83.2
6.1c	110	121	6	(0.456)	2.12	0.06124	3.18	0.03613	5.66	647.7 ± 67.0	228.8 ± 12.7	− 32.5
6.2c	161	218	9	1.542	0.53	0.04995	2.04	0.03834	2.31	192.7 ± 46.7	242.6 ± 5.5	
7.1c	281	232	15	(0.202)	7.17	0.08851	1.74	0.03662	5.66	1393.6 ± 33.0	231.9 ± 12.9	− 73.4
911-1 Granosyenite												
1.1r	329	464	23	(0.263)	7.23	0.10210	1.52	0.04192	2.01	1662.6 ± 27.8	264.7 ± 5.2	− 76.8
2.1c	355	320	23	(0.169)	11.29	0.13930	1.02	0.04085	2.02	2218.5 ± 17.5	258.1 ± 5.1	− 84.8
3.1c	275	314	15	0.760	0.39	0.05400	1.66	0.03773	2.02	371.0 ± 36.9	238.8 ± 4.7	− 11.3
4.1c	775	757	41	1.058	0.16	0.05082	1.11	0.03856	2.11	232.7 ± 25.4	243.9 ± 5.1	
4.1r	1319	1134	68	(0.162)	3.81	0.07991	1.33	0.03881	2.02	1194.8 ± 25.9	245.4 ± 4.9	− 71.5
5.1c	2207	1590	119	(0.234)	2.13	0.06817	0.61	0.04066	2.02	873.7 ± 12.6	256.9 ± 5.1	− 66.6
6.1c	182	137	9	0.857	0.45	0.05028	2.15	0.03794	2.06	208.0 ± 49.0	240.0 ± 4.8	
7.1c	261	298	15	(0.211)	6.65	0.09682	2.06	0.03792	2.02	1563.7 ± 38.1	239.9 ± 4.8	− 73.6
8.1c	227	297	13	1.235	0.19	0.05125	2.02	0.03902	2.01	252.1 ± 45.8	246.8 ± 4.9	
9.1c	308	412	18	(0.553)	1.55	0.06016	1.56	0.03851	2.02	609.3 ± 33.3	243.6 ± 4.8	− 44.2
10.1c	550	1093	35	1.817	0.34	0.05134	1.29	0.03819	2.03	256.1 ± 29.3	241.6 ± 4.8	
10.1r	1026	521	55	0.140	4.91	0.08461	1.42	0.04053	2.26	1306.6 ± 27.4	256.1 ± 5.7	− 72.3
11.1c	622	783	34	0.769	2.72	0.05457	1.61	0.03752	2.02	394.6 ± 35.6	237.5 ± 4.7	− 17.2
12.1c	332	473	19	1.485	0.21	0.05105	1.60	0.03847	2.03	243.1 ± 36.4	243.3 ± 4.9	
9113-4 Syenite												
1.1c	338	580	21	1.511	2.00	0.05154	3.59	0.03915	3.65	265.1 ± 80.3	247.6 ± 8.9	
2.1c	229	250	12	1.167	0.16	0.05047	1.70	0.03796	3.62	216.7 ± 38.8	240.2 ± 8.5	
3.1c	436	605	25	1.221	0.15	0.05162	1.31	0.03824	3.62	268.6 ± 29.7	241.9 ± 8.6	
4.1c	356	389	20	1.416	0.29	0.04996	1.38	0.03957	3.62	193.1 ± 31.7	250.1 ± 8.9	
5.1c	249	247	13	1.036	0.09	0.05076	1.89	0.03963	3.62	229.9 ± 43.0	250.6 ± 8.9	
6.1c	225	376	14	1.341	0.21	0.05231	1.73	0.03961	3.62	299.0 ± 38.9	250.4 ± 8.9	
7.1c	582	811	35	1.451	0.08	0.05090	1.54	0.04046	3.63	236.3 ± 35.2	255.7 ± 9.1	
8.1c	421	548	25	1.271	0.17	0.05128	1.54	0.04062	3.62	253.4 ± 34.9	256.7 ± 9.1	
9.1c	436	491	24	1.037	0.14	0.05148	1.65	0.03920	3.62	262.4 ± 37.5	247.9 ± 8.8	
10.1c	419	611	25	2.020	0.14	0.04950	1.80	0.03941	3.63	171.6 ± 41.5	249.2 ± 8.9	
11.1c	267	248	14	0.689	0.12	0.05295	1.65	0.03909	3.62	326.7 ± 37.0	247.2 ± 8.8	

Analyses were performed on a high-mass resolution, high-sensitivity Cameca IMS 1270 ion-microprobe at the NORDSIM facility in Stockholm, Sweden. Analyses from cores denoted by "c" and from mixed zones or rims by "r." Data are reported at 1σ. Errors in age estimates are quoted at 1σ. All ages are calculated using the decay constants of Steiger and Jager (1977). Pb concentrations determined prior to correction for common Pb. Th/U ratios calculated from $^{207}Pb/^{206}Pb$ and $^{208}Pb/^{206}Pb$ ages: ratios in parentheses differ significantly from measured Th and U concentrations. Ages reported in parentheses are not included in mean age determinations (see text). Disc. (%) refers to the degree of discordance at the 2σ error limit between $^{207}Pb/^{206}Pb$ and $^{206}Pb/^{238}U$ ages.

magmatic source for these rocks. The distributions of trace and RE elements (Figs. 3 and 4) show high Ba and elevated Ta and Nb, which are typical of granitoids formed in a within-plate setting (Pearce et al., 1984). The high Ce and Sm abundance in Fig. 4 suggest a considerable role for crustal assimilation.

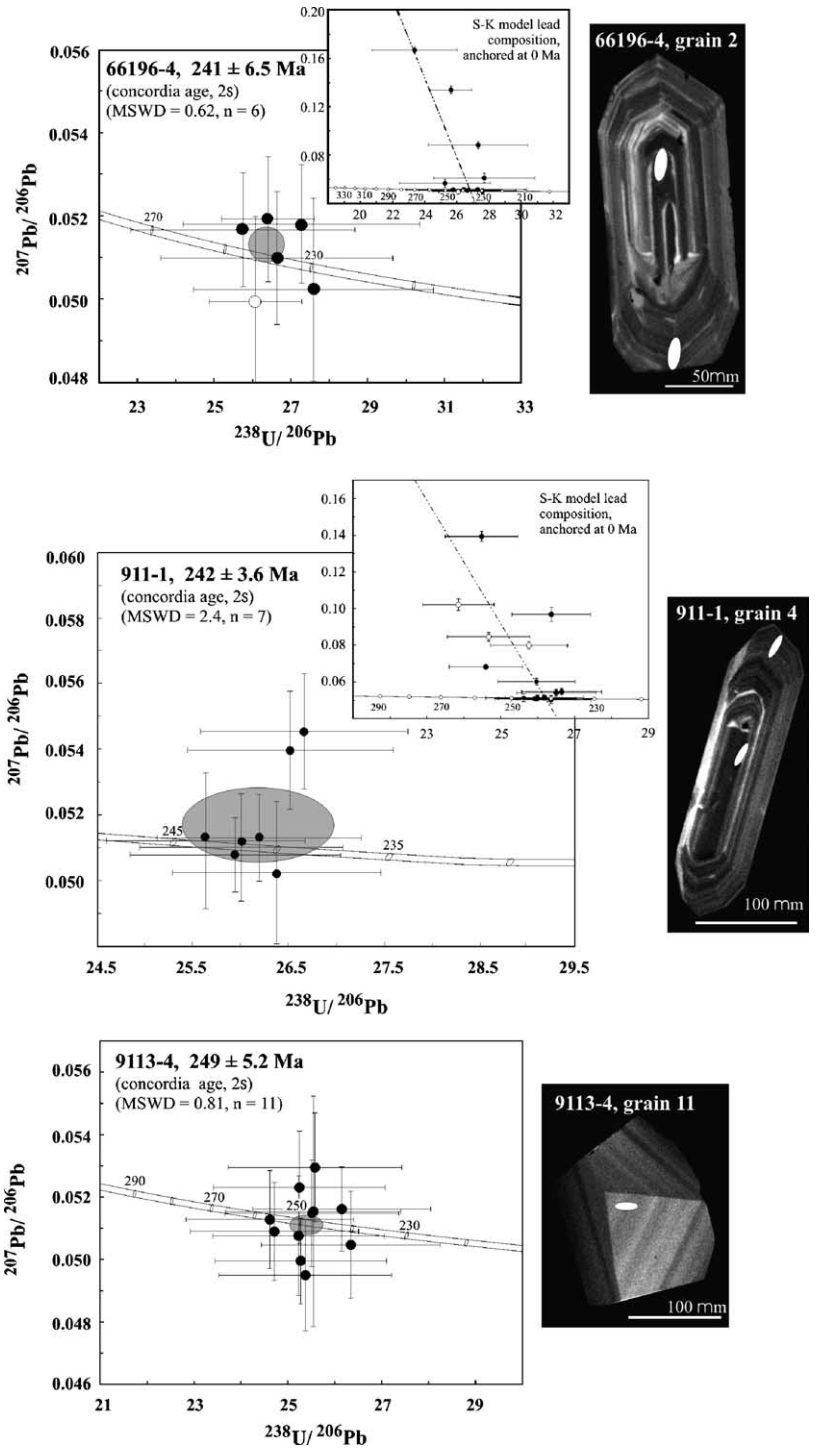

Fig. 5. Concordia diagrams with cathodoluminesence zircon images for samples 66196-4, 911-1 and 9113-4. Spot analyses from the cores of zircon grains are represented by black ovals, rims or mixed zones by white ovals. The final concordia ages are shown in gray.

Although we have analyzed only four samples from the syenite–granite bodies, they all appear to be characterized by similar trace and RE element distributions. Assuming that the samples are representative of the bodies as a whole, we tentatively conclude that they represent the product of a common magmatic source of mixed crustal and mantle origin.

5. Isotope geochemistry

5.1. U–Th–Pb analyses

U–Th–Pb analyses were performed with the Cameca IMS 1270 ion-microprobe (Swedish Museum of Natural History, Stockholm, Sweden). Analytical procedures are similar to those described by Whitehouse et al. (1997, 1999). Analytical data from syenogranite, syenite and syenite–porphyry are presented in Table 2. Concordia diagrams (Tera and Wasserburg, 1973, 1974) with cathodoluminescence images are shown in Fig. 5. All three samples generated concordia ages (Ludwig, 1998), which are reported at the 2σ confidence level. The ion beam was oval and ca. 25 μm in its long dimension.

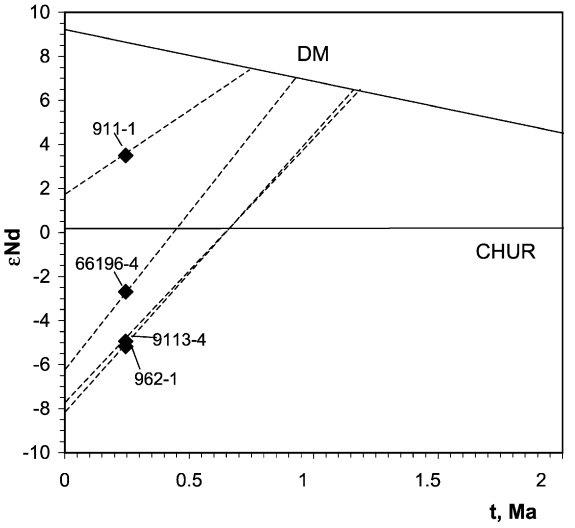

Fig. 6. ε_{Nd}–t diagram for Early Triassic granitoids from northwest Taimyr.

Eight to twelve grains (including cores and rims) were analyzed in each sample, resulting in 11–14 analyses per sample. In one sample (9113-4), the zircon was pink, in the other samples the zircon was golden. A single population of transparent, euhedral to subhedral, stubby (aspect ratio, 1:1 to 1:3) zircon grains was present in each sample. Cathodo-

Table 3
Rb, Sr, Sm and Nd isotopic contents from Early Triassic granitoids of northwestern Taimyr

Sample	U–Pb age (Ma)	$^{87}Rb/^{86}Sr$	$^{87}Sr/^{86}Sr$	Error ($\times 10^{-5}$) 2σ	$(^{87}Sr/^{86}Sr)_0$	$^{147}Sm/^{144}Nd$	$^{143}Nd/^{144}Nd$	$\varepsilon_{Nd}(0)$	$\varepsilon_{Nd}(t)$	t_{Nd}DM (Ma)
962-1	245	0.31917	0.70681	15	0.70582	0.09969	0.51222	−8.212	−5.18	1174
9113-4	245	0.2082	0.70709	21	0.70644	0.10382	0.51224	−7.842	−4.94	1192
66196-4	245	0.67561	0.70682	18	0.70472	0.08854	0.51223	−6.067	−2.69	932
911-1	245	0.63062	0.70780	23	0.70584	0.14143	0.51273	1.775	+3.5	761.9

Chemical separation and mass spectrometric analyses were done at the Laboratory of Isotope Geology, Naturhistoriska Riksmusett, Stockholm. Rb, Sr, Sm and Nd were separated by standard chromatographic ion-exchange procedures (Ludwig, 1991). Decay constants follow the convention of Steiger and Jager (1977). Isotopic ratios were determined on a Finnigan MAT 261 mass spectrometer equipped with multiple Faraday cups and run multidynamically. Rb and Sr were determined by ICP-MS method using VG Element PQ2 ICP-MS mass spectrometer (Table 1). The $^{87}Rb/^{86}Sr$ ratios were calculated using the measured $^{87}Sr/^{86}Sr$ ratios and determined concentrations of Rb and Sr. Error associated with $^{87}Rb/^{86}Sr$ ratios is $\sim \pm 3\%$ (2σ). External precision $^{87}Sr/^{86}Sr$ ratios is $\sim \pm 0.01\%$. Replicate analyses of unspiked USGS BCR1 standard yielded $^{87}Sr/^{86}Sr$ ratios indistinguishable from the accepted value of Gladney et al. (1990) and no further correction was applied. Initial $^{87}Sr/^{86}Sr$ ratios $(^{87}Sr/^{86}Sr)_i$ were calculated by correcting for the amount of ^{87}Sr produced by ^{87}Rb decay since the formation of the rock. Decay constants follow the convention of Steiger and Jager (1977) and Lugmair and Marti (1978). Rb and Sr are listed in Table 1. Sm and Nd contents were determined by isotope dilution (Table 1). Error on $^{147}Sm/^{144}Nd$ ratios is less than 0.1%. Error on $^{143}Nd/^{144}Nd$ is less than 0.002%. Replicate analyses of La Jolla standard yielded $^{143}Nd/^{144}Nd$ ratios somewhat lower (0.511826 ± 0.000023, 2σ) than the accepted value of 0.511854. Consequently, a correction factor of +0.000028 has been applied to all analyses. ε_{ND} parameters were calculated relative to CHUR (Jacobsen and Wasserburg, 1984); the depleted mantle model age t_{Nd}DM assumes the model of DePaolo et al. (1991).

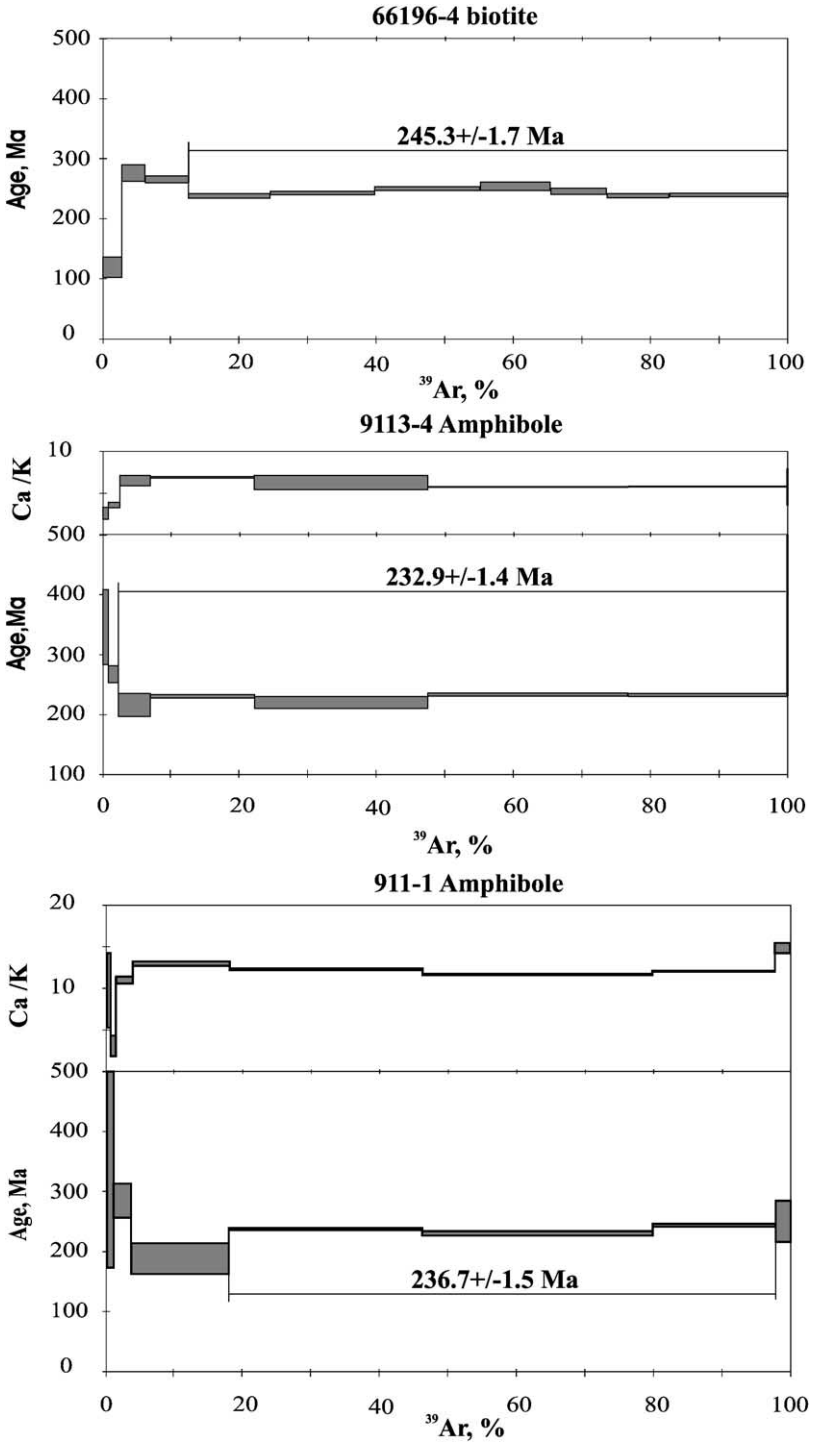

Fig. 7. Ar/Ar ages for biotite and amphibole from subalkaline granitoids of northwest Taimyr.

luminescence images of all grains showed typical igneous, oscillatory growth zoning. Most analyses define a concordia age from 249 to 241 Ma. A linear regression through each data set, using the model lead composition of Stacey and Kramers (1975) anchored to 0 Ma, yields an intercept age statistically indistinguishable from the concordia age. We, therefore, interpret the concordia ages to represent the time of formation (crystallization age) of the syenogranite and syenite.

5.2. Sm–Nd and Rb–Sr isotopes

The syenite and granite are characterized by variable Nd and Sr isotopic compositions, and ε_{Nd} values ranging from −5.18 to +3.5 (Table 3). These data point to the hybrid character of the parental magma(s). In the $\varepsilon_{Nd}-t$ diagram (Fig. 6), given that the samples are all the same age, the subparallel trends of Nd evolution indicate simultaneously both the similarity of their sources and the considerable assimilation of a crustal component by the melt. Negative ε_{Nd} values support a key role for a crustal component. The positive ε_{Nd} value, together with the relatively low $^{87}Sr/^{86}Sr$ ratio of 0.704–0.706, reflects the important influence of mantle components. The maximum model source ages ($t_{Nd}DM = 1174–1192$ Ma) correspond to the maximum negative ε_{Nd} (−5.18 and −4.94). The younger model ages from 932 to 761 Ma correspond to the positive and small negative ε_{Nd} values. The fact that all the model ages are Proterozoic probably

Table 4
Argon isotopic analytical data

Temperature (°C)	$^{36}Ar/^{40}Ar$	$^{36}Ar/^{40}Ar$ error	$^{39}Ar/^{40}Ar$	$^{39}Ar/^{40}Ar$ error	Cumulative percent ^{39}Ar	$^{40}Ar^{*}$ (%)	Age (Ma)	Age (Ma) error
66196-4 Biotite, 11.5 mg, J= 0.003265 ± 0.000028, total gas age: 243.8 ± 2.3 Ma								
600	0.00176	0.00023	0.02288	0.00023	2.4	47.9	119.2	16.7
700	0.00063	0.00014	0.01606	0.00014	6.0	81.3	276.0	13.8
750	0.00008	0.00006	0.02006	0.00006	12.4	97.4	265.7	5.3
800	0.00028	0.00003	0.02120	0.00003	24.4	91.6	238.2	3.1
850	0.00014	0.00003	0.02169	0.00003	39.6	95.8	243.2	3.0
900	0.00014	0.00003	0.02105	0.00002	55.3	95.9	250.3	2.8
950	0.00031	0.00008	0.01959	0.00007	65.5	90.7	254.0	6.5
1000	0.00035	0.00006	0.02003	0.00006	73.7	89.6	246.0	5.2
1050	0.00029	0.00004	0.02115	0.00003	82.8	91.5	238.5	3.3
1100	0.00015	0.00002	0.02191	0.00002	100	95.4	240.0	2.6
9113-4 Amphibole, 36.8 mg, J= 0.003058 ± 0.000024, total gas age: 231.5 ± 15.4 Ma								
700	0.00240	0.00019	0.00418	0.00019	0.6	29.0	347.0	61.7
900	0.00191	0.00008	0.00835	0.00007	2.4	43.6	267.4	13.6
950	0.00131	0.00098	0.01464	0.00098	7.0	61.2	217.2	20.0
1000	0.00162	0.00001	0.01166	0.00002	22.1	52.2	231.5	2.5
1050	0.00072	0.00073	0.01838	0.00073	47.4	78.6	221.7	10.0
1100	0.00042	0.00002	0.01929	0.00002	76.5	87.6	234.5	2.2
1150	0.00104	0.00002	0.01535	0.00002	99.9	69.2	233.1	2.6
1200	0.00327	0.00003	0.00022	0.00003	100	3.3	695.5	188.6
911-1 Amphibole, 34.7 mg, J= 0.003357 ± 0.000029, total gas age: 230.5 ± 4.5 Ma								
500	0.00318	0.00013	0.00046	0.00013	0.1	6.0	374.1	374.1
800	0.00202	0.00083	0.00548	0.00083	1.2	40.4	398.5	224.8
900	0.00192	0.00016	0.00854	0.00016	3.7	43.4	284.0	28.5
1000	0.00226	0.00015	0.01019	0.00015	17.8	33.3	187.6	24.4
1050	0.00126	0.00001	0.01503	0.00001	46.1	62.8	236.9	2.1
1100	0.00068	0.00003	0.01968	0.00003	79.9	79.8	230.1	2.9
1150	0.00154	0.00002	0.01262	0.00002	97.9	54.3	243.4	3.0
1200	0.00212	0.00019	0.00839	0.00019	100	37.3	250.6	34.9

reflects assimilation of lower crustal rocks of this age in the magma.

5.3. Ar–Ar isotope analyses

$^{40}Ar/^{39}Ar$ analyses of biotite and amphibole were performed using the Micromass 5400 static mass spectrometer (United Institute of Geology, Geophysics and Mineralogy, Novosibirsk, Russia). Mineral separates >0.15 mm in size were wrapped in Al foil and vacuum sealed in quartz vials. Irradiation was performed under Cd-shielding in the VEK-11 carrier of the VVR-K research reactor at the Tomsk Polytechnical Institute (Russia). K/Ar biotite standard MCA-11 was used between every two samples for neutron gradient monitoring, and the neutron gradient did not exceed 0.5%. $^{40}Ar/^{39}Ar$ step heating experiments (Table 4; Fig. 7) were accomplished using a quartz vial heated by an external furnace. The ^{40}Ar blank at 1200 °C measured over a period of 40 min did not exceed 5×10^{-9} STP. Released argon was doubly purified by exposure to Ti and ZrAl SAES getters.

The $^{40}Ar/^{39}Ar$ ages from biotite and amphibole range between 245 and 233 Ma and define the time of closure of the K–Ar isotopic system. These ages indicate the time at which the intrusions cooled ~ 550–500 °C for amphibole and to ~ 350–300 °C for biotite. For the Uboininsky massif (sample 66196-4), U–Pb and Ar–Ar data show the same ages within errors, indicating rapid cooling. For syenite from the Rastorguev Island (sample 9113-4), $^{40}Ar/^{39}Ar$ ages from amphibole are ca. 15 Ma younger than ages obtained by U–Th–Pb method. It is unlikely that this small high-level massif cooled over a prolonged interval, so this $^{40}Ar/^{39}Ar$ age may reflect postmagmatic processes.

6. Discussion

The U–Pb zircon results lead us to conclude that emplacement of the western Taimyr syenite–granite stocks took place in a short interval between ~ 249 and 241 Ma (with errors in the range of ± 6.5–3.6 Ma). These plutonic rocks intrude mafic extrusive and intrusive rocks of the Siberian traps, the oldest of which is dated at 251.2 ± 0.3 Ma (Kamo et al., 1996). Thus, the syenite–granite plutons formed coeval with or a few million years after the trap magmatism. A very similar series of events has been described for the Emeishan large igneous province in southwestern China, where the main phase of flood basalt magmatism took place at 259 ± 3 Ma (Zhou et al., 2002), and a later phase of felsic magmatism represented by syenite was emplaced at 254.6 ± 1.3 (Lo et al., 2002).

Petrographic and geochemical features of subalkaline rocks from northwestern Taimyr (granites, syenites and syenite–porphyries) allow us to classify them as mafic A-type granitoids. These rocks crystallized from high-temperature, little differentiated melts, depleted in H_2O and enriched in fluorine under low-pressure conditions.

Despite the limited number of samples, the similar distributions of trace and RE elements, and the similar petrographic characteristics indicate the commonality of this plutonic series. The high contents of trace and rare-earth LIL elements, and the positive ε_{Nd} are typical for melts formed from an undepleted mantle source. At the same time, the HREE content, the wide ε_{Nd} variations from positive to negative values, and the intermediate mantle–crustal Sr_i values for these rocks point to a hybrid character. A similar hybrid origin is typical for trap provinces, as well as for other 'hot spot' sources, which are often formed from the mixing of depleted mantle, undepleted mantle, and continental crust (Kuz'min, 1985; Lightfoot et al., 1993; Dobretsov and Kirdyashkin, 1998; Kempton et al., 2000; Xu et al., 2001; Lo et al., 2002).

With respect to the formation of the early Triassic subalkaline plutons from Taimyr, our data suggest that mantle and continental crustal components were mixed in variable proportions. This conclusion is in accord with data indicating that these intrusions are very similar in age to the time of the main stage of Siberian trap magmatism, i.e., 251–249 Ma (Dalrymple et al., 1995; Kamo et al., 1996). Syenite from Rastorguev Island is characterized not only by negative ε_{Nd} values, testifying to a substantial crustal contribution, but also by a high model age ($t_{Nd}DM$) of 1200 Ma. Significantly younger model ages ($t_{Nd}DM = 932–761$ Ma) were obtained for the rocks from the Uboininsky and Morzhovsky massifs. It is interesting that the model ages determined for these latter massifs are close to those for Permian (264 Ma) postcollisional granitoids from Taimyr (Vernikovsky et al., 1998, 1999). These results are in accord with

the hypothesis of Dobretsov (1997) that alkaline granitoid magmatism occurs in peripheral zones surrounding plumes in continental crust that has not yet cooled following collisional orogenic processes. As noted earlier, similar alkaline granitoids at the boundary of the Permian and Triassic have been described for accretionary–collisional complexes in Central Asia, where they frame the Siberian superplume to the south (Jahn et al., 1990; Yarmolyuk et al., 1997).

In conclusion, these new geochronological and geochemical data for early Triassic syenite–granite stocks from Taimyr provide important information on magmatic events associated with the Permo-Triassic northern Eurasian superplume. However, additional petrological and geochemical study are required to test these preliminary conclusions resulting from our limited sample population and data set, and to further evaluate the links with the Siberian trap magmatism.

Acknowledgements

We thank N. Dobretsov for insightful comments, support and many discussions; and T. Rivers for his informal review and for suggesting improvements to the manuscript. The constructive reviews of L. Johansson and G. Fershtater greatly improved the early version of this paper. We thank E. Bulgakova, N. Dmitrieva and A. Yasenev for preparing the graphics and tables. Analytical work received financial support from INTAS and the Russian Foundation of Basic Research (grants IR-97-1139; 01-05-64732; 00-15-98562). This is NORDSIM publication no. 68.

References

Basu, A.R., Poreda, R.J., Renne, P.R., Teichmann, F., Vasiliev, Y.R., Sobolev, N.V., Turin, B.D., 1995. High ^{3}He plume origin and temporal–spatial evolution of the Siberian flood basalts. Science 269, 822–825.

Bezzubtsev, V.V., Zalyaleev, R.Sh., Goncharov, Y.I., 1986. Geological map of Mountain Taimyr, scale 1:500 000. Explanatory notes, Krasnoyarsk (in Russian).

Bogdanov, N.A., Khain, V.Ye., Rosen, O.M., Shipilov, E.V., Vernikovsky, V.A., Drachev, S.S., Kostyuchenko, S.L., Kuz'michev, A.B., Sekretov, S.B., 1998. Explanatory notes for the Tectonic Map of the Kara and Laptev Seas and Northern Siberia (scale 1:2 500 000). Moscow, Institute of the Lithosphere of Marginal Seas of RAS.

Campbell, I.H., Czamanske, G.K., Fedorenko, V.A., Hill, R.I., Stepanov, V., 1992. Synchronism of the Siberian Traps and the Permian–Triassic Boundary. Science 258, 1760–1763.

Claoué-Long, J.C., Zichao, Z., Guogan, M., Shaohua, D., 1991. The age of the Permian–Triassic boundary. Earth Planet. Sci. Lett. 105, 182–190.

Collins, W.J., Beams, S.D., White, A.J.R., Chappell, B.W., 1982. Nature and origin of A-type granites with particular reference to Southeastern Australia. Contrib. Mineral. Petrol. 80, 189–200.

Dalrymple, G.B., Czamanske, G.K., Fedorenko, V.A., Simonov, M.A., Lanphere, M.A., Likhachev, A.P., 1995. A reconnaissance ^{40}Ar/^{39}Ar geochrologic study of ore-bearing and related rocks, Siberian Russia. Geochim. Cosmochim. Acta 59, 2071–2083.

DePaolo, D., Linn, A., Schubert, G., 1991. The continental crustal age distribution: methods of determining mantle separation age from Sm–Nd isotopic data and application to the southwestern United States. J. Geophys. Res. 96, 2071–2088.

Dobretsov, N.L., 1997. Permian–Triassic magmatism and sedimentation in Eurasia as a result of a superplume. Doklady Earth Sciences 354 (4), 497.

Dobretsov, N.L., Kirdyashkin, A.G., 1998. Deep-Level Geodynamics Balkema, Rotterdam.

Dobretsov, N.L., Vernikovsky, V.A., 2001. Mantle plumes and their geological manifestations. Int. Geol. Rev. 43, 771–787.

Egiazarov, B.Kh., 1959. Geological structure of Severnaya Zemlya Archipelago. Tr. NIIGA 94 Leningrad (in Russian).

Evensen, N.M., Hammilton, P.S., O'Nions, R.K., 1978. Rare-earth abundances in chondritic meteorites. Geochim. Cosmochim. Acta 42, 1199–1212.

Gladney, E., Jones, E., Nickell, E., 1990. 1988 compilation of elemental concentration data for U.S.G.S. basalt BCR-1. Geostand. Newsl. 14, 209–359.

Jacobsen, S., Wasserburg, G., 1984. Sm–Nd isotopic evolution of chondrites and achondrites: II. Earth Planet. Sci. Lett. 67, 137–150.

Jahn, B.M., Zhou, X.H., Li, J.L., 1990. Formation and tectonic evolution of Southeastern China and Taiwan: isotopic and geochemical constraints. Tectonophysics 183, 145–160.

Kamo, S.L., Czamanske, G.K., Krough, T.E., 1996. A minimum U–Pb age for Siberian flood-basalt volcanism. Geochim. Cosmochim. Acta 60, 3505–3511.

Kempton, P.D., Fitton, J.G., Saunders, A.D., Nowell, G.M., Taylor, B.S., Hardarson, B.S., Pearson, G., 2000. The Iseland plume in space and time: a Sr–Nd–Pb–Hf study of the North Atlantic rifted margin. Earth Planet. Sci. Lett. 177, 255–271.

Kuz'min, M.I., 1985. Geochemistry of magmatic rocks from Phanerozoic mobile belts. Novosib. Nauka (in Russian).

Lightfoot, P.C., Hawkesworth, C.J., Hergt, J., Naldrett, A.J., Gorbachev, N.S., Fedorenko, V.A., Doherty, W., 1993. Remobilisation of the continental lithosphere by a mantle plume: major-, trace-element, and Sr-, Nd-, and Pb-isotope evidence from picritic and tholeiitic lavas of the Noril'sk District, Siberian Trap, Russia. Contrib. Mineral. Petrol. 114, 171–188.

Lo, C.-H., Chung, S.-L., Lee, T.-Y., Wu, G., 2002. Age of the Emeishan flood magmatism and relations to Permian–Triassic boundary events. Earth Planet. Sci. Lett. 198, 449–458.

Ludwig, K.R., 1991. PbDAT for MS-DOS, version 1.21. U. S. Geol. Surv., Open-File Report 88-542, 35 pp.

Ludwig, K.R., 1998. On the treatment of concordant uranium–lead ages. Geochim. Cosmochim. Acta 62, 665–676.

Lugmair, G.W., Marti, K., 1978. Lunar initial $^{143}Nd/^{144}Nd$: differential evolution of the lunar crust and mantle. Earth Planet. Sci. Lett. 35, 273–284.

Pearce, J.A., Harris, N.B.W., Tingle, A.G., 1984. Trace element discrimination diagrams for the tectonic interpretation of granitic rocks. J. Petrol. 25, 956–983.

Pogrebitsky, Yu.E., 1971. Paleotectonic analysis of Taimyr folded area. Tr. NIIGA 166 Nedra. Leningrad (in Russian).

Price, J.D., Hogan, J.P., Gilbert, M.C., London, D., Morgan, G.B., 1999. Titanite–fluorite equilibria in the A-type Mount Scott Granite: a means for assessing F contents of felsic magma. Fourth Hutton Symposium Abstracts: The Origin of Granites and Related Rocks. Clermont-Ferrand, France, p. 239.

Ravich, M.G., Chaika, L.A., 1956. Differentiated intrusion of trap formation from Taimyr folded area. Izv. AN SSSR, Ser. Geol. 1, 50–64 (in Russian).

Ravich, M.G., Chaika, L.A., 1959. Small intrusions from Byrranga Range (Taimyr peninsula). Tr. NIIGA 88 Leningrad (in Russian).

Renne, P.R., Zichao, Z., Richards, M.A., Black, M.T., Basu, A.R., 1995. Synchrony and causal relations between Permian–Triassic boundary crises and Siberian Flood Volcanism. Science 269, 1413–1416.

Shand, S.J., 1943. Eruptive Rocks. Wiley, London, New York.

Sharma, M., 1997. Siberian traps. In: Mahoney, J.J., Coffin, M.F. (Eds.), Large Igneous Provinces: Continental, Oceanic, and Planetary Flood Volcanism, Geophysical Monograph, vol. 100, 273–295.

Sharma, M., Basu, F.R., Nesterenko, G.V., 1992. Temporal Sr-, Nd-, and Pb-isotopic variations in the Siberian flood basalts: implications for the plume-source characteristics. Earth Planet. Sci. Lett. 113, 365–381.

Stacey, J., Kramers, J., 1975. Approximation of terrestrial lead isotope evolution by a two-stage model. Earth Planet. Sci. Lett. 26, 207–221.

Steiger, R.N., Jager, E., 1977. Convention on the use decay constants in geo-and cosmochronology. Earth Planet. Sci. Lett. 36, 359–362.

Tera, F., Wasserburg, G., 1973. A response to a comment on U–Pb systematics in lunar basalts. Earth Planet. Sci. Lett. 19, 213–217.

Tera, F., Wasserburg, G., 1974. U–Th–Pb systematics on lunar rocks and inferences about lunar evolution and the age of the Moon. Proceedings of the 5th Lunar Scientific Conference. Geochim. Cosmochim. Acta Suppl. 5, vol. 2, 1571–1599.

Vakar, V.A., 1962. Trapp formation of TaimyrPetrography of East Siberia, vol. 1 Izd. AN SSSR, Moscow, pp. 256–340 (in Russian).

Vernikovsky, V.A., 1995. Riphean and Paleozoic complexes of the Taimyr Foldbelt: condition of formation. Petrology 3, 55–72.

Vernikovsky, V.A., 1996. Geodynamic evolution of the Taimyr fold area: Novosibirsk, Siberian Branch. Russ. Acad. Sci. (in Russian).

Vernikovsky, V.A., Neimark, L.A., Ponomarchuk, V.A., Vernikovskaya, A.E., 1995. Geochemistry and age of collision granitoids and metamorphites of the Kara microcontinent (Northern Taimyr). Russ. Geol. Geophys. 36, 46–60.

Vernikovsky, V.A., Sal'nikova, E.B., Kotov, A.B., Ponomarchuk, V.P., Kovach, V.P., Travin, A.V., Yakovleva, S.Z., Berezhnaya, N.G., 1998. The age of postcollision granitoids of the North Taimyr: U–Pb, Sm–Nd, Rb–Sr and Ar–Ar data. Doklady Earth Sciences 363A (9), 1191.

Vernikovsky, V.A., Kovach, V.P., Kotov, A.B., Vernikovskaya, E.B., Sal'nikova, E.B., 1999. Sources of granitoids and the evolutionary stages of the continental crust. Geochem. Int. 37 (6), 493–503.

Vladimirov, A.E., Nikulov, L.P., 1991. Paleogeographic and paleontological reconstruction of beginning trap volcanism in West Taimyr. Paleovolcanism in Altay–Sayan Folded Area and Siberian Platform. Nauka, Novosibirsk, pp. 104–109 (in Russian).

Whitehouse, M., Claesson, S., Sunde, T., Vestin, J., 1997. Ion-microprobe U–Pb zircon geochronology and correlation of Archean gneisses from the Lewisian Complex of Gruinard Bay, northwestern Scotland. Geochim. Cosmochim. Acta 61, 4429–4438.

Whitehouse, M., Kamber, B., Moorbath, S., 1999. Age significance of U–Th–Pb zircon data from early Archean rocks of west Greenland—a reassessment based on combined ion-microprobe and imaging studies. Chem. Geol. 160, 201–224.

Xu, Y., Chung, S.-L., Jahn, B.-M., Wu, G., 2001. Petrologic and geochemical constraints on the petrogenesis of Permian–Triassic Emeishan flood basalts in southwestern China. Lithos 58, 145–168.

Yarmolyuk, V.V., Vorontsov, A.A., Kovalenko, V.I., Zhuravlev, D.Z., 1997. Isotopic inhomogeneity of source of Late Paleozoic intraplate magmatism in Central Asia. Russ. Geol. Geophys. 38, 1178–1183.

Zhou, M.-F., Malpas, J., Song, X.-Y., Robinson, P.T., Sun, M., Kennedy, A.K., Lesher, C.M., Keays, R.R., 2002. A temporal link between the Emeishan large igneous province (SW China) and the end-Guadalupian mass extinction. Earth Planet. Sci. Lett. 196, 113–122.

Zolotukhin, V.V., 1990. Features of Tulay–Kiryaka Differentiated Intrusion from Taimyr Nauka, Novosibirsk (in Russian).

Zolotukhin, V.V., 1998. The heat effect of trap injection on the Siberian Platform in the context of the plume concept. Russ. Geol. Geophys. 39, 1061–1065.